Raman spectra of $Ge_xAs_ySe_{1-x-y}$ glasses

R. P. Wang,[a] A. Smith, A. Prasad, D. Y. Choi, and B. Luther-Davies
Laser Physics Centre, Research School of Physics and Engineering, Australian National University, Canberra, Australian Capital Territory 0200, Australia

(Received 22 February 2009; accepted 21 July 2009; published online 26 August 2009)

Various Ge–As–Se glasses spanning a mean coordination number (MCN) from 2.2 to 2.94 have been investigated using differential scanning calorimetry and Raman spectroscopy. The glass transition temperature T_g was found to increase with increasing MCN, except for those glasses located within the nanoscale phase-separated region of the phase diagram. The evolution of Raman features at wavenumbers from 150 to 350 cm^{-1} exhibits two transitionlike features. Merging of the 225 and 250 cm^{-1} modes at MCN=2.5 is a symbol of the extinction of Se–Se bonds. Additionally, the appearance of two modes at 280–290 and 170 cm^{-1} at MCN>2.7 come from the defect modes of ethanelike $Ge_2Se_{6/2}$. The increase in the scattering from these defects is an important factor leading to enhanced optical loss in the glasses with high MCN. © *2009 American Institute of Physics*. [DOI: 10.1063/1.3204951]

I. INTRODUCTION

The mean coordination number (MCN; defined as a sum of the respective elemental concentrations times their covalent coordination number) for a glass network is an important parameter that measures network connectivity, and it has been found that many physical properties of glasses correlate with MCN.[1–10] This is especially evident for Ge–As–Se chalcogenide glasses with covalent coordination numbers of four, three, and two, respectively. Phillips[9] and Thorpe[10] first identified a floppy-to-rigid transition at MCN=2.4 by mean field theory using constraint counting algorithm. By considering self-organization of a random network, Boolchand further found a rigid but stress-free intermediate phase by Raman spectra and temperature-modulated differential scanning calorimetry (TMDSC).[6–10] A thermally reversing compositional window was reported in the intermediate phase, where the glasses are generally nonaging.[4–8] Nonaging behavior makes the glasses very interesting for photonics applications since structural relaxation observed in most amorphous materials is detrimental to the stability of all photonic devices.[11] Recently, we reported investigations of the linear and nonlinear optical properties of Ge–As–Se bulk glasses.[12] We found that high third order nonlinearity can be achieved in two compositional ranges for glasses containing either low (0%–15%) Ge or high (>35%) Ge. While the high Ge content glasses had high glass transition temperatures, they also displayed elevated levels of optical loss that correlated with the increasing number of defect bonds identified from Raman spectra. Interestingly we concluded the best compositions for photonic applications corresponded to Ge concentrations of around 10%–15% with MCN of around 2.47, which places the glasses directly in the stress-free rigid intermediate phase mentioned above.

For Ge–As–Se ternary glasses a widely used structural model involves tetrahedral $GeSe_{4/2}$ and pyramidal $AsSe_{3/2}$ units cross-linked by Se-chain fragments in a stochastic fashion.[4] Theoretical predictions and experimental measurements of the glass transition temperature T_g are consistent for glasses with low Ge and As concentrations but diverge for those with high Ge and As concentrations. The deviation is thought to be due to randomness in the bonding between local structural units being replaced by extended range structural correlations.[4] Raman vibrational frequencies of corner-sharing $GeSe_{4/2}$ units in $Ge_xAs_xSe_{1-2x}$ glasses as a function of the chemical composition show three distinct power laws, supporting the existence of three different phases in the Ge–As–Se ternaries. The intermediate phase therefore was identified at MCN from 2.27 to 2.46.[7] However, all evidence collected previously came from the glasses with the same Ge and As concentrations. Further experiments for a wide compositional range are necessary to elucidate the correlation between the network structure, the physical properties, and MCN.

In this paper, we investigated a series of Ge–As–Se glasses spanning a MCN from 2.2 to 2.94. We measured T_g and Raman scattering spectra of each glass. After assigning the peaks to the particular vibrations and decomposing the experimental spectra based on these assignments, we tried to address two questions: how do the vibrational modes evolve with changing MCN and what is the correlation of the microstructure with the optical loss in the glasses?

II. EXPERIMENTS

Chalcogenide glasses were typically prepared from 50 g batches of high purity (5*N*) germanium, arsenic, and selenium metals. The required amounts of these raw materials were weighed inside a dry nitrogen glovebox and loaded into a precleaned quartz ampoule. The loaded ampoule was dried under vacuum (10^{-6} Torr) at 110 °C for 4 h to ensure removal of surface moisture from the raw materials. The ampoule was then sealed under vacuum using an oxygen hydrogen torch and introduced into a rocking furnace for melting of the contents at 900 °C. The melt was homogenized for a period of not less than 30 h; then the ampoule was removed

[a]Electronic mail: rpw111@rsphysse.anu.edu.au.

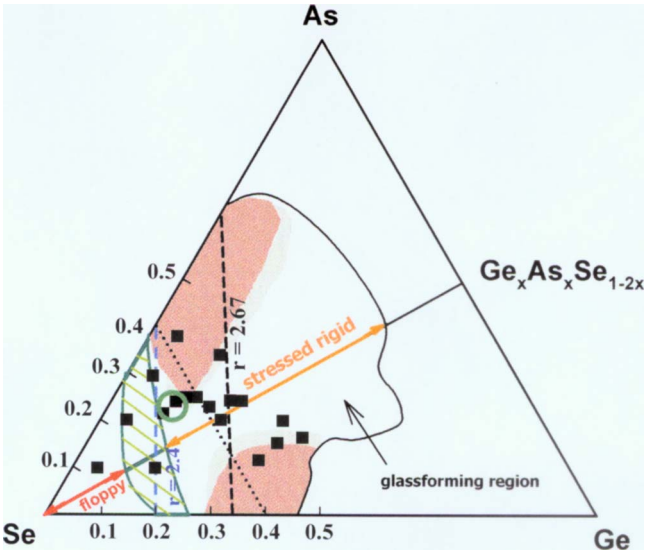

FIG. 1. (Color online) All our samples are marked in phase diagram of Ge–As–Se ternary glasses. The original phase diagram is provided by Professor Punit Boolchand. The intermediate phase is shown by the hashed region between the floppy and the stressed rigid phases. Nanophase-separated regions are shown by gray shading. Our best compositions with high nonlinearity and low optical loss are located at the green circle.

from the rocking furnace at a predetermined temperature and air quenched. The resulting glass boule was subsequently annealed at a temperature 30 °C below the glass transition temperature T_g, then slowly cooled to room temperature. Following the annealing process, the glass boules were sectioned to form disks of 25 mm diameter and approximately 2 mm thick. The disks had opposite surfaces ground plane parallel and then polished to optical quality. Polished samples were visually inspected for internal defects and striae. Only samples free from defects and striae were used in the Raman scattering measurements.

The glass transition temperature T_g was measured using a differential scanning calorimeter (Shimadzu DSC-50) with 10 K/min scanning rate, and no devitrification or crystallization was observed for the samples in this study. In total, we prepared 18 glasses with different compositions as labeled in Fig. 1. These glasses cover all the regions in the phase diagram including floppy, intermediate, and stressed rigid phases and the regions where nanoscale phase separation occurs. All Raman spectra were recorded in the backscattering geometry using a custom micro-Raman system. The emission from an 808 nm single mode diode laser was filtered using a pair of 808 nm notch filters (Semrock LL01-808) to eliminate amplified spontaneous emission (ASE) before being focused onto the sample using a ×40 objective. The scattered light collected was passed through a long pass edge filter (Semrock LP02-808RU) into a QE65000 scientific-grade spectrometer with a spectral resolution of ≈3 cm^{-1} (Ocean Optics) and a Hamamatsu charged-coupled devices detector. The laser power at the sample was <800 μW, and the intensity did not exceed 2 kW/cm^2, leading to a typical integration time of 5 s for all spectra. We measured the spectra of both fresh and samples after 20 min of laser radiation using different laser powers. When no difference between these two spectra was apparent, we considered that any photoinduced effects were totally suppressed.

TABLE I. A list of the prepared samples, ordered by compositions, MCN, T_g, and whether Se is rich or poor in the samples.

Composition	MCN	T_g (°C)	Se-rich
$Ge_5As_{10}Se_{85}$	2.2	133.5	Yes
$Ge_5As_{20}Se_{75}$	2.3	145.2	Yes
$Ge_5As_{30}Se_{65}$	2.4	179.5	Yes
$Ge_{15}As_{10}Se_{75}$	2.4	179.3	Yes
$Ge_{11}As_{22}Se_{67}$	2.44	210.5	Yes
$Ge_{11.5}As_{24}Se_{64.5}$	2.47	236.7	Yes
$Ge_5As_{38}Se_{57}$	2.48	224.9	No
$Ge_{12.5}As_{25}Se_{62.5}$	2.5	247.9	Chemical stoichiometry
$Ge_{15}As_{25}Se_{60}$	2.55	280.4	No
$Ge_{18}As_{23}Se_{59}$	2.59	293.4	No
$Ge_{22}As_{20}Se_{58}$	2.64	323.7	No
$Ge_{15}As_{34}Se_{51}$	2.64	285.9	No
$Ge_{22}As_{24}Se_{54}$	2.68	335.9	No
$Ge_{24}As_{24}Se_{52}$	2.72	353.1	No
$Ge_{33}As_{12}Se_{55}$	2.78	383.3	No
$Ge_{35}As_{15}Se_{50}$	2.85	404.3	No
$Ge_{33}As_{20}Se_{47}$	2.86	405.2	No
$Ge_{39}As_{16}Se_{45}$	2.94	386.5	No

III. RESULTS AND DISCUSSION

Table I lists all the glass compositions and T_g. It is clear that T_g gradually increases with increasing MCN, except for the samples of $Ge_5As_{38}Se_{57}$, $Ge_{15}As_{34}Se_{51}$, and $Ge_{39}As_{16}Se_{45}$. These samples are all located within the nanoscale phase separation region of the phase diagram for the Ge–As–Se ternary glass. The appearance of phase separation can destroy the backbone of the network and consequently cause a decrease in T_g.[4,6] It is well established that T_g depends on the connectivity and thus on the rigidity of the vitreous network.[13,14] Therefore increasing the concentration of Ge and As will result in a vitreous matrix with higher T_g. Noteworthy is that in Table I, the glasses with same MCN of 2.4 exhibit almost the same T_g, emphasizing that T_g does depend on the network connectivity and hence MCN rather than the particular chemical composition.

The typical Raman spectra of the glasses are shown in Fig. 2. The energy range of vibrations for all samples is nearly the same and extends to around 330 cm^{-1}. This indicates the similarity in mass and bond forces among these three elements. The general features of these spectra include (1) an asymmetric peak around 250 cm^{-1} present in $Ge_5As_{10}Se_{85}$ and which gradually broadens with increasing Ge and As concentrations; (2) a peak at 190 cm^{-1}, which appears in all the samples and increases in intensity with increasing Ge concentration; and (3) an obvious shoulder appearing in the low wavenumber region around 170 cm^{-1} becomes dominant in $Ge_{39}As_{16}Se_{45}$, and also a broad feature at 220–270 cm^{-1} for low MCN glasses extends to high wavenumbers around 300 cm^{-1} for high MCN glasses.

Since Ge–Se and As–Se units are basic blocks to build Ge–As–Se glass network, we start from the individual vibra-

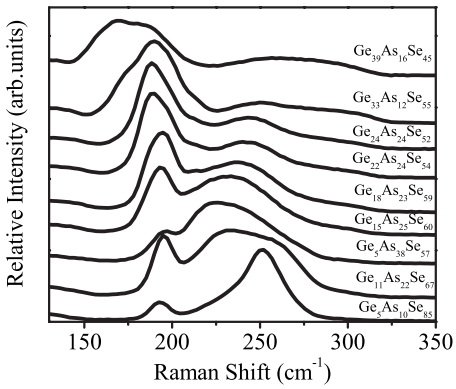

FIG. 2. Raman spectra of the typical glasses without the application of Bose–Einstein correction. The spectra are shifted along the *y*-axis in sequence from low to high MCN for clarification.

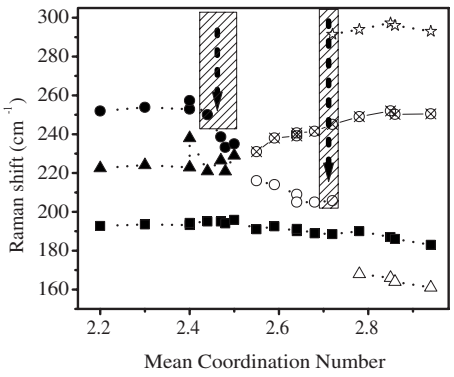

FIG. 4. Raman vibrational modes as a function of MCN. The different symbols represent different Raman vibrational modes that are described in the text. The shaded frames with the arrows indicate the regions of two transitionlike features.

tional modes of Ge–Se and As–Se glasses. For Ge_xSe_{1-x}, Tronc *et al.*[15] reported that the 250 cm^{-1} peak is connected to the Se–Se bonds. With increasing Ge concentration, two peaks appear at 195 and 213 cm^{-1}, which could be due to the vibrational modes in the corner-sharing and the edge-sharing $GeSe_{4/2}$ tetrahedra, respectively.[15,16] One peak at 175 cm^{-1} and another peak at 300 cm^{-1} for $Ge_{40}Se_{60}$ sample were also reported from the ethanelike modes.[15,17,18] Regarding As_xSe_{1-x}, Boolchand reported two principal modes of $AsSe_{3/2}$ pyramidal units at 225 and 243 cm^{-1} for As_2Se_3, and As_4Se_4 monomers could appear in As_xSe_{1-x} when $x>0.50$.[19] These As_4Se_4 monomers are very stable in the glassy state.[13] In $Ge_yAs_ySe_{1-2y}$ containing equal concentrations of Ge and As, Mamedov *et al.*[19] anticipated that once *y* exceeded the chemical threshold, homopolar As–As and Ge–Ge bonds emerged as part of the backbone, therefore increasing the connectivity. Trends in T_g that continues to increase even when MCN exceeds 2.6 were considered as evidence to support this postulate.

We decomposed the spectra into several Gaussian curves, and the typical results are shown in Fig. 3. Here we emphasize that although we decomposed the broadbands at high wavenumber in Se-poor samples into several Gaussian components, it is quite conceivable that a larger number of vibrational modes contribute to the overall spectrum. However, due to the similarity of the atomic radii and weight of Ge, As, and Se atoms because of their proximity in the periodic table, replacing one by another does not lead to a significant shift in the vibrational frequencies. Instead, such substitution will just broaden the bands in the amorphous phase. Therefore, it is almost impossible to decompose the spectra with any meaning into a larger number of Gaussian components. For the same reason, the intensity of the decomposed peaks is not discussed in this paper.

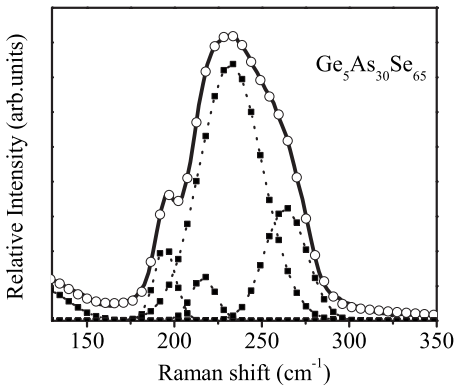

FIG. 3. The decomposed Raman spectrum for $Ge_5As_{30}Se_{65}$ sample. The solid line is the experimental data, the open circles are the fitting spectrum, and the square-and-dotted lines are the decomposed Raman peaks.

The decomposed Raman vibrational frequencies are shown in Fig. 4. On the basis of the reports mentioned above, we ascribe the peak at 190 cm^{-1} to the corner-sharing vibrational mode of $GeSe_{4/2}$ tetrahedral (solid squares in Fig. 4), 225 cm^{-1} to the mode of $AsSe_{3/2}$ pyramidal unit (solid triangles in Fig. 4), and 250 cm^{-1} to Se–Se bond (solid circles in Fig. 4) since it clearly appears in a Se-rich sample such as $Ge_5As_{10}Se_{85}$. The corner-sharing 190 cm^{-1} vibrational mode of $GeSe_{4/2}$ tetrahedral is almost constant when MCN is less than 2.5 but slightly decreases to low wavenumber when MCN is more than 2.5. The 225 cm^{-1} mode in $AsSe_{3/2}$ pyramidal unit and 250 cm^{-1} of Se–Se vibration can be seen in the MCN below 2.5, and then these two modes merge into 240 cm^{-1}. The disappearance of 250 cm^{-1} peak at MCN of $\approx$2.5 for $Ge_{12.5}As_{25}Se_{62.5}$ can be considered due to the complete consumption of Se by Ge and As in this nominally stoichiometric sample.

With any further increase in MCN, there will not be enough Se to form $GeSe_{4/2}$ and $AsSe_{3/2}$; therefore the existence of Se–Se bonds is almost impossible. However, two vibration modes appear: one increases from 240 to 250 cm^{-1} (open cross-circles in Fig. 4) with increasing MCN to 2.94, and another decreases from 220 to 205 cm^{-1} (open circles in Fig. 4) with increasing MCN and mixes with corner-sharing 190 cm^{-1} mode at MCN=2.7. In addition, at MCN>2.7, the feature at 250 cm^{-1} gradually transforms into a broadband extending to 300 cm^{-1} (open five stars in Fig. 4), and another shoulder appear at 170 cm^{-1} (open triangles in Fig. 4). Based on $\sim$4 kcal/mol difference between the bonding energies of Ge–Se and As–Se (Ref. 13) and the difference in the electronegativity from Se(2.48) to As(2.18) and Ge(2.01),[20] we argue that $AsSe_{3/2}$ units will be first destroyed. Part of Se in $AsSe_{3/2}$ units will be replaced by As or Ge. Since As and Ge elements are lighter than Se, the sub-

stitution will induce a slight upshift in the Raman peaks as evident in Fig. 4 for the peaks at 240–250 cm^{-1}. Moreover, such gradual change in Raman peaks at 240–250 cm^{-1} indicates that the pyramidal structure is still maintained with increasing substitution. On the other hand, Raman peaks at 220–210 cm^{-1} could be due to the edge-sharing $GeSe_{4/2}$ tetrahedral since the position is close to the reported value.[6]

We assigned the 175 and 290 cm^{-1} peaks to ethanelike $Ge_2Se_{6/2}$ vibrational modes at MCN=2.7, where much rigid Ge–Ge bonds will be formed followed by As–As or As–Ge bonds as mentioned above on the basis of bonding energies and electronegativity arguments. In addition, we do not observe any sharp Raman peaks of As_4Se_4 as shown in Ref. 5; therefore we conclude that no significant amount of the $AsSe_{4/4}$ structure exists in these glasses. This is consistent with the evolution of T_g except for those samples in nanophase-separated regions where the independent As_4Se_4 monomers could cut fully polymerized backbones, leading to a maximum value of T_g.[4]

These data identify two transition regions centered on MCN≈2.45 and MCN≈2.7 as indicated in Fig. 4. The positions of these transition regions are in good agreement with our recent measurements of the MCN dependence of the elastic moduli of $Ge_xAs_ySe_{1-x-y}$ glasses, which identified transition thresholds at MCN=2.45 and 2.65, respectively.[21] Transitions at the same MCN values have also been identified in the dependence of the linear refractive index; the material density and the band gap of these same glasses.[22] Our data, therefore, correlate well with the models of Thorpe[10] and Tanaka[2] who predicted transitions from a floppy-to-rigid network and rigid to stressed rigid network at MCN=2.4 and MCN=2.67, respectively. The position of the low MCN transition that we identify appears, however, to occur at higher MCN than that reported for the $As_xGe_xSe_{1-2x}$ ternary system[6] from TMDSC and attributed as a transition from floppy to the so-called Boolchand intermediate phase. In that absence of TMDSC for the glasses, we have studied that it is difficult to relate our results to those in Ref. 6, although it is conceivable that the position and width of any thermally reversing window would change because of the different chemical environment in our glasses.

Nevertheless, while the high optical loss in the glasses including high Ge is due to increasing scattering of the defects bonds such as Ge–Ge, Ge–As, and As–As in the network, the best compositions with both high nonlinearity and low optical loss are those compositions with MCN of around 2.47, which are located at the green circle and are outside of the intermediate phase in $Ge_xAs_xSe_{1-2x}$ glasses, as shown in Fig. 1. If the best compositions are correlated with the Boolchand intermediate phase, the present results indicate that the intermediate phase should extend to a wide region in $Ge_xAs_ySe_{1-x-y}$ glasses.

IV. CONCLUSIONS

In summary, we have investigated a series of Ge–As–Se glasses spanning a MCN range from 2.2 to 2.9. We found that T_g gradually increases with increasing MCN, except for those glasses located in the nanoscale phase-separated region in the phase diagram. The vibrational features were found to change with increasing MCN. The corner-sharing 190 cm^{-1} vibrational mode of $GeSe_{4/2}$ tetrahedral is almost constant when MCN is less than 2.5 but slightly decreases to low wavenumber when MCN is more than 2.5. The 225 cm^{-1} mode and the 250 cm^{-1} Se–Se bond vibration can be seen in the MCN below 2.5, and then these two modes merge to a single feature at 240 cm^{-1}. Additionally, two modes appear for high MCN samples, one is located at 280–290 cm^{-1} and another at 170 cm^{-1} when MCN increases to 2.7. These two peaks are thought to be related to the defect modes of ethanelike $Ge_2Se_{6/2}$, which are a main factor to induce large optical loss in the glasses with high MCN.

ACKNOWLEDGMENTS

We thank Professor Punit Boolchand who provided us an electronic version of phase diagram for GeAsSe ternary glasses. This research was partly supported by the Australian Research Council through its Centres of Excellence and Federation Fellow Programs.

[1] M. Tatsumisago, B. L. Halfpap, J. L. Green, S. M. Lindsay, and C. A. Angell, Phys. Rev. Lett. **64**, 1549 (1990).
[2] K. Tanaka, Phys. Rev. B **39**, 1270 (1989).
[3] R. Bohmer and C. A. Angell, Phys. Rev. B **45**, 10091 (1992).
[4] Y. Wang, P. Boolchand, and M. Micoulaut, Europhys. Lett. **52**, 633 (2000).
[5] F. Wang, S. Mamedov, P. Boolchand, B. Goodman, and M. Chandrasekhar, Phys. Rev. B **71**, 174201 (2005).
[6] T. Qu, D. G. Georgiev, P. Boolchand, and M. Micoulaut, Mater. Res. Soc. Symp. Proc. **754**, CC8.1.1 (2003).
[7] S. Chakravarty, D. G. Georgiev, P. Boolchand, and M. Micoulaut, J. Phys.: Condens. Matter **17**, L1 (2005).
[8] P. Boolchand, G. Lucovsky, J. C. Phillips, and M. F. Thorpe, Philos. Mag. **85**, 3823 (2005).
[9] J. C. Phillips, J. Non-Cryst. Solids **34**, 153 (1979).
[10] M. F. Thorpe, J. Non-Cryst. Solids **57**, 355 (1983); M. F. Thorpe, D. J. Jacobs, M. V. Chubynsky, and J. C. Phillips, *ibid.* **266–269**, 859 (2000).
[11] R. P. Wang, A. V. Rode, S. J. Madden, C. J. Zha, R. A. Javis, and B. Luther-Davies, J. Non-Cryst. Solids **353**, 950 (2007).
[12] A. Prasad, C. J. Zha, R. P. Wang, A. Smith, S. Madden, and B. Luther-Davies, Opt. Express **16**, 2804 (2008).
[13] M. A. Popescu, *Non-Crystalline Chalcogenides* (Kluwer, Dordrecht, 2001).
[14] R. P. Wang, C. J. Zha, A. V. Rode, S. J. Madden, and B. Luther-Davies, J. Mater. Sci.: Mater. Electron. **18**, 419 (2007).
[15] P. Tronc, M. Bensoussan, A. Brenac, and C. Sebenne, Phys. Rev. B **8**, 5947 (1973).
[16] M. Stevens, P. Boolchand, and J. G. Hernandez, Phys. Rev. B **31**, 981 (1985).
[17] N. Kumagai, J. Shirafuji, and Y. Inuishi, J. Phys. Soc. Jpn. **42**, 1262 (1977).
[18] K. Jackson, A. Briley, S. Grossman, D. V. Porezag, and M. R. Pederson, Phys. Rev. B **60**, R14985 (1999).
[19] S. Mamedov, D. G. Georgiev, T. Qu, and P. Boolchand, J. Phys.: Condens. Matter **15**, s2397 (2003).
[20] R. P. Wang, D. Y. Choi, A. V. Rode, S. J. Madden, and B. Luther-Davies, J. Appl. Phys. **101**, 113517 (2007).
[21] R. P. Wang, A. Smith, B. Luther-Davies, H. Kokkonen, and I. Jackson, J. Appl. Phys. **105**, 056109 (2009).
[22] D. A. P. Bulla, R. P. Wang, A. Prasad, A. V. Rode, S. J. Madden, and B. Luther-Davies, Appl. Phys. A: Mater. Sci. Process. **96**, 615 (2009).